https://doi.org/10.20965/ijat.2018.p0413

Paper:

Development of a Straight Fibers Pneumatic Muscle

Francesco Durante[*,†], **Michele Gabrio Antonelli**[*], **Pierluigi Beomonte Zobel**[*], **and Terenziano Raparelli**[**]

[*]DIIIE, University of L'Aquila
Via Giovanni Gronchi 18, 67100 L'Aquila, Italy
[†]Corresponding author, E-mail: francesco.durante@univaq.it
[**]DIMEAS, Politecnico di Torino, Torino, Italy
[Received October 4, 2017; accepted February 28, 2018]

This paper presents the development and implementation of a pneumatic muscle actuator based on an idea proposed by a research group at the University of Warsaw. The muscle comprises a silicone rubber tube with plugs at the ends. The tube wall contains high-rigidity wires arranged parallel to the tube axis. Circular rings are present on the exterior of the tube. When air is introduced into the tube, the actuator becomes bulky and contracts. In order to establish a prediction model of muscle behavior, a finite element model was developed, and in this model, the Mooney-Rivlin formulation was implemented with two coefficients for rubber simulation and truss elements for the wires. Several prototypes were developed, and a test bench for the experimental characterization of muscle performance was set up. The results of comparison between prototype behavior and model prediction are presented. The finite element model can be used to design the actuator with different dimensions; hence, it was used to conduct a simulated test campaign to develop a quick actuator sizing procedure. Using dimensional analysis, few project parameters were identified on which the performance of the actuator depends. Through a complete simulation campaign using the finite element model, an abacus was constructed. It allows sizing the actuator as required based on the desired performances according to an established procedure.

Keywords: pneumatic muscle, finite element modeling, non-linear behavior, design procedure

1. Introduction

The traditional pneumatic actuators have been widely used in industrial processes because of the main features of air: simple availability, clean functioning, and low cost as compared to the electrical and hydraulic technologies. Traditional pneumatic actuators have a high power-to-weight ratio. However, because of the compressibility of air, position and force control is not easy. In industrial processes, the difficulty in position control does not impose a limitation: two position actuators are commonly used to achieve cycles with high frequencies, high repeatability, high speed, and high durability.

On the contrary, this control cannot be neglected in biomedical applications [1, 2], especially in bio-inspired [3] or collaborative robotics [4], where humans share a workspace with a robot [5], and where the presence of rigid moving components could be dangerous for the human operator. In such applications, pneumatic actuators must have high compliance, intrinsic safety, and a high power-to-weight ratio.

Pneumatic muscle actuators (PMAs) can overcome these problems. PMAs are made of a highly elastic deformable membrane equipped with a reinforcing structure: the air inlet inside the membrane allows for the deformation of the latter, constrained by the reinforcing structure, resulting in the development of a force: an axial contraction of the membrane leads to a pulling force, while an axial expansion leads to a pushing force.

Since 1950, several types of PMAs were developed. The first one was the McKibben muscle (MKM) [6–10], which is a braided muscle. MKM is commercially available as Rubbertuator manufactured by Bridgestone Rubber Company, MAS and DMSP fluidic muscles of Festo AG, and Shadow Air Muscles of Shadow Robot Company. Other types of PMAs are as follows: the netted muscle [11], embedded muscle [12, 13], pleated muscle [14, 15], bellow muscle [16–19], and straight fiber muscle (SFM) [20].

The SFM, which is the subject of the present study, comprises a rubber tube equipped with high stiffness wires axially placed within the wall of the tube. The ends of the tube and of the wires are connected to end caps or to tendon-like components that must guarantee mechanical and pneumatic sealing. The air inlet inside the tube causes a radial bulging of the tube; axial contraction occurs because of the inextensibility of the wires due to the high stiffness. In order to restrain radial bulging, several equidistant rings are placed along the external surface of the tube, dividing the muscle in segments. The behavior of each segment of the muscle is identical, as shown in **Fig. 1**.

Several studies were carried out on MKMs: theoretical modeling was conducted, and experimental relations

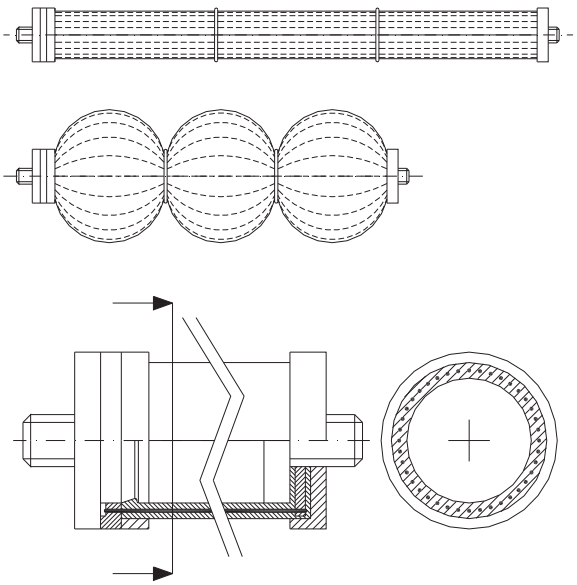

Fig. 1. Schematic of a straight fiber muscle. In this case, two external rings are adopted to limit the lateral bulging, dividing the muscle into three segments. The wall contains 40 glass fiber wires.

were established in terms of effects of the rounding of the terminal ends [21–23]; the fatigue life [24, 25], maximum contraction [6], and force prediction [9, 26] were defined; finite element models were developed to study and validate the nonlinear behavior of the McKibben muscle and to establish a quantitative design method [27–29]; several applications for rehabilitation, robotics, and wearable devices were developed using McKibben muscles as power actuators [30–35].

However, few studies were carried out on the SFM, which was first proposed in 1970 [36]. Experimental comparisons between the MKM and the SFM were carried out in [37]; theoretical and experimental comparisons between the same muscle types and modeling of the SFM were performed in [38]. Recently, a theoretical comparison between the same muscle types was carried out using models of the static characteristics of both types of muscles [39]. A robot for rehabilitation of the upper limb used four pairs of SFMs, mounted in an agonistic-antagonistic mode [40].

A numerical model and an experimental prototype of an SFM are presented in this paper. The behavior of the SFM is strongly nonlinear owing to the nonlinear constitutive law of the rubber [41] of the tube and owing to the geometrical nonlinearity caused by the high deformation of the muscle during its functioning. Therefore, developing a predictive analytical model of the muscle behavior is a complicated task; hence, a numerical model was developed. The numerical model is a finite element model. After the model was experimentally validated, it was used to develop a practical design procedure for the muscle. The procedure, based on a single correlation graph using three-dimensional parameters, was developed by a dimensional analysis.

2. Pneumatic Muscle

The muscle studied in this work is based on the idea proposed by a Warsaw University Research Group [36], with some differences in the design of the heads. The tube is made of a silicone rubber [41]. The wires are made of fiberglass, which has been used in different prototypes [42]. The development of a numerical model can be useful both for optimizing the actuator without using numerous prototypes and for defining a practical dimensioning procedure for this type of actuators [43].

2.1. Numerical Model

The first idea for the model was to employ a three-dimensional geometry; however, this geometry requires a long time for geometric modeling.

As the model is considered a project or optimization tool, modeling time is an important parameter. Therefore, a plane model with axisymmetric constrains was considered. The tube and the heads have an axisymmetric geometry, while the wires are not a continuum and are finite in number.

The wires in the circumferential direction do not cause any structural effects, and they are theoretically axially inextensible. In the circumferential direction, only the structural effects due to the rubber are observed. An axisymmetric model can be considered by modeling the wires as a line of truss elements with axial stiffness equivalent to the total stiffness of all the wires in the rubber tube. With regard to this equivalence, in general, the axial stiffness of the truss element is defined using two parameters: the Young's modulus and the cross-sectional area. As the axisymmetric model is represented by the radial cross section of the muscle, it is possible to insert only one line of truss elements. Hence, the truss elements in the model were considered to have the same Young's modulus as that of the used material (glass fiber) and to have the cross-sectional area of one wire (diameter 0.75 mm) multiplied by 40, which is the total number of wires used in the prototype.

The dimensions of the prototypes were adopted as the model dimensions. The tube was modeled by 72 elements with three elements in the radial direction. The heads were modeled using 4-node flat elements, and the wires, using 24 truss-type elements.

The results obtained using the axisymmetric model were compared with the three-dimensional model that models all of the 40 wires exactly. The two models are perfectly equivalent for the predictions, and hence, in the continuation of the research, the axisymmetric model was used. **Fig. 2** shows the results of the comparison between the two models.

In order to define a deep field of validity of the numerical model, muscles with three and four segments and muscles with different Φ_0/L_{m0}, i.e., resting diameter on resting muscle length, ratios were considered. The outer rings were modeled by radial constraints.

The models were used to simulate three isotonic and

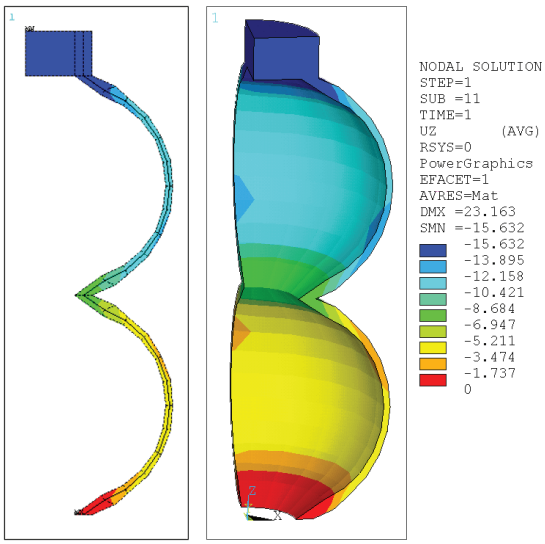

Fig. 2. Three-dimensional and axisymmetric models of a four-segment pneumatic muscle.

isometric characterization tests by considering different constraint and load conditions.

Isotonic tests are constant force tests, during which the muscle is free to contract: the contraction is detected versus the internal pressure for different applied loads. Isometric tests consist of constant contraction tests. The muscle is maintained at constant length by means of constraints, and the force is measured versus the internal pressure for different values of contraction.

The properties of the material of the heads, i.e., aluminum, were obtained from literature; for the rubber that constitutes a critical aspect of the model, experimental characterization was carried out in the laboratory.

Preliminary tests of the model were carried out with a structural solid plane element with four nodes for the heads and for the tube. The element formulation is linear and it was possible to observe only linear behavior for the rubber. Therefore, accurate results were obtained only for true deformation values up to 50% (while prototypes reached deformations up to 180%). Other tests were carried out by implementing the Blatz-Ko hyperelastic model, but this model too did not yield satisfactory results. Finally, the first-order Mooney-Rivlin model was implemented with a hyperelastic element for rubber simulation. The constitutive law of the material, shown in **Fig. 3**, was obtained by experimental measurements through a cylindrical test and by using 18 measuring points across the entire deformation range.

These data were used to derive the two constants that characterize the first-order Mooney-Rivlin model. Their values are $C_{10} = 0.0694$ and $C_{01} = 0.0628$.

The specimen diameters were measured during the tests to allow estimation of the Poisson modulus based on volume variations. The wires, in the model, are characterized by the Young modulus of the glass fibers of 70000 MPa.

Figure 4 shows examples of model simulation for isometric and isotonic tests.

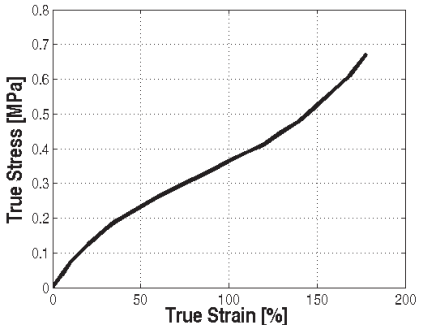

Fig. 3. Experimental σ-ε curve.

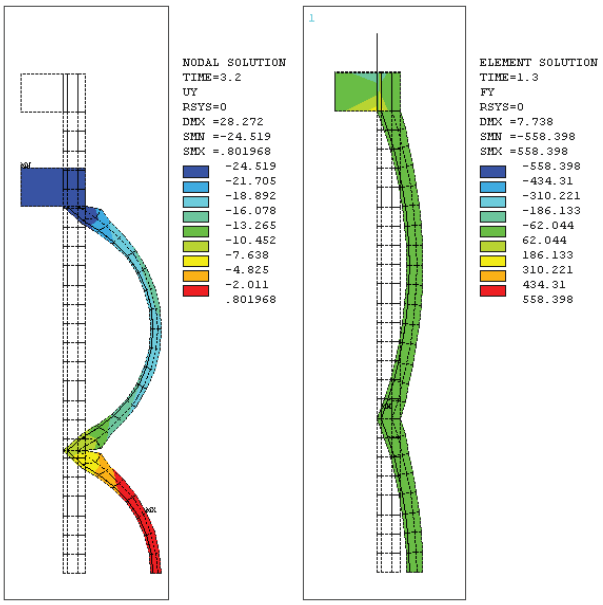

Fig. 4. Examples of outputs of three-segment models for the isotonic and isometric simulations.

2.2. Experimental Activity

The experimental process is divided into four parts: design and implementation of a bench for producing prototype actuators; realization of prototypes; design and realization of a bench for experimental tests; and experimental tests for the characterization of prototypes. For the bench for realizing the actuators, a process employing an aluminum core on which threaded rings are mounted for wire application was developed. The core was placed inside a mold for forming the tube.

The silicone material was cast, and after solidification, the tube was obtained with the wires in the wall and internal rings for anchoring the heads. A two-component silicone with high deformability and resistance was chosen for the rubber. The design parameters for the muscle are listed in **Table 1**. They were so chosen as to allow fitting 40 threads inside the wall along the circumference. A pneumatic fitting placed on a head allowed feeding and discharging air to the muscle. **Fig. 5** shows photographs of the prototype muscle with the three segments at rest and in two deformed configurations.

Table 1. Main dimensions of the muscle prototype.

Tube length	External diameter	Tube thickness	f. glass threads diameter
250 mm	34 mm	6 mm	0.75 mm

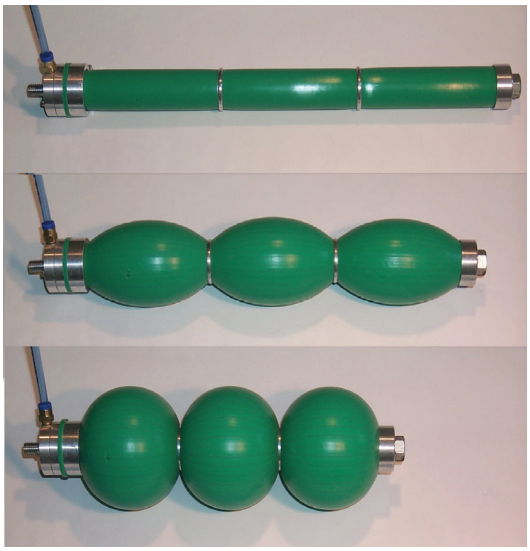

Fig. 5. Three-segment muscle prototype.

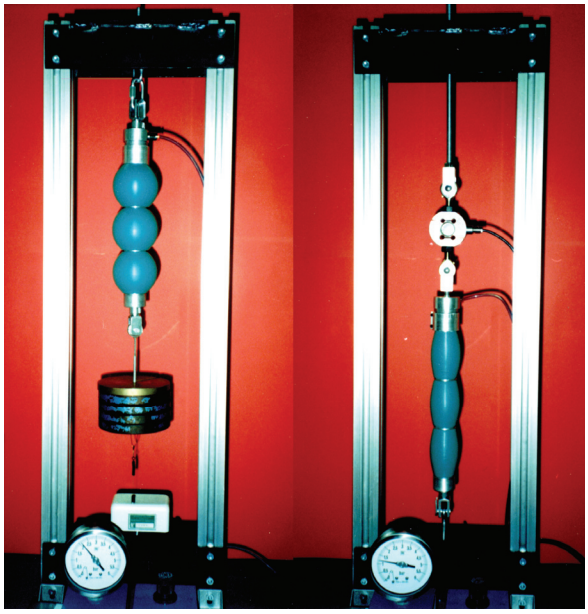

Fig. 6. Experimental test bench with the 3-segment muscle (1): isotonic (left) and isometric (right) tests.

Finally, the experimental test bench was prepared. The bench had a portal structure, and it allowed conducting static and dynamic tests.

The test bench for isotonic and isometric tests allows detection of muscle strength or contraction and pressure. The bench was equipped with a PC-based data acquisition system with a data acquisition card and 16-bit digital-to-analog converter, a pressure sensor (maximum pressure 1 MPa), a load cell (maximum load 1000 N), and a linear position sensor based on an electric resistance transducer. A pressure regulator was connected to the compressed air line of the laboratory. **Fig. 6** shows the testbed with the configurations for the isotonic and isometric tests. The isotonic tests were conducted as follows: the muscle was hung from one end, and at the other end, a mass was hung; subsequently, compressed air was injected into the muscle.

During the experimental test, muscle shortening was recorded as a function of pressure. The pressure in the tests was increased from zero to the maximum value of 0.22 MPa through quasistatic configurations.

In the isometric tests, one extremity of the muscle was blocked at the bottom of the test bench, and the other end was connected to a load cell suspended from the top bar of the test bench. During the test muscle force was recorded as a function of pressure.

2.3. Comparison Between the Numerical Model and Experimental Prototype

As mentioned above, to develop the numerical model, the σ-ε relationship of the elastomeric material should be known. The same test bench that was used for muscle characterization was used to characterize the material.

Model validation was carried out by drawing up a plan of isotonic and isometric experimental tests.

The procedure for validating the model is as follows:

- Acquisition of the σ-ε curve of the elastomeric material.
- Acquisition of experimental curves; contraction versus pressure in the isotonic tests under three load conditions, namely, 10 N, 80 N and 150 N and force-dependent pressure for three contraction values, namely, 0%, 7.2%, and 14.4%.
- Calculation of the curves using the numerical model under the same conditions as those in the experimental tests.
- Comparison of the results of the simulations and experimental tests.

In the isotonic experiments, the exact loads are 9.6 N for the 10-N test, 80.7 N for the 80-N test and 148.8 N in the 150-N test.

The procedure was iterative and was used to optimize the behavior of the model by considering several parameters: constraints, element formulation, mesh density, and the amount of experimental data for constructing the σ-ε relationship of the elastomeric material.

Figures 7 and **8** show a comparison of the results obtained with the optimized muscle model with the prototype performance in the isotonic and isometric tests.

For the isotonic curves, the constant load applied at one extremity of the muscle, namely, 10 N, 80 N and 150 N is a parameter. For the isometric curves, the muscle contraction at which the constraint becomes active on the length

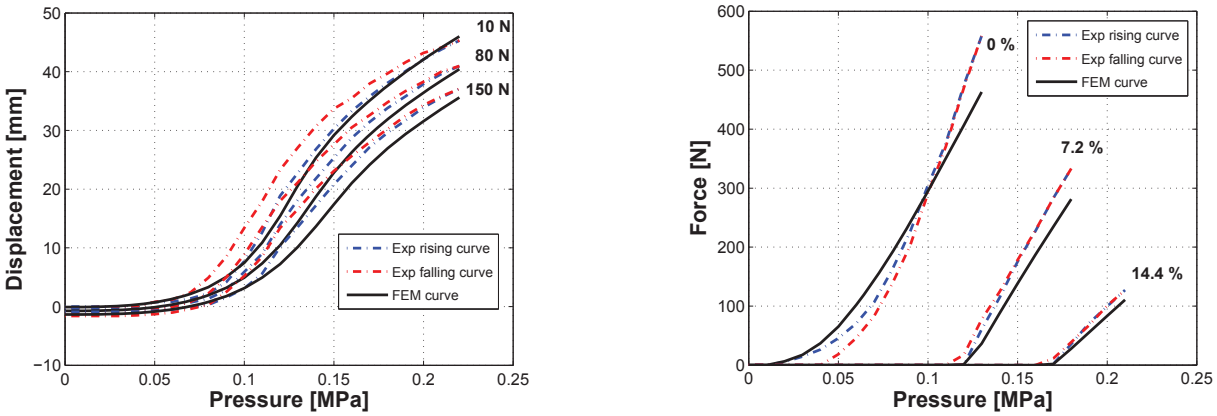

Fig. 7. Comparison between the behaviors of the experimental prototype and the finite element model for the three-segment muscle: isotonic and isometric tests.

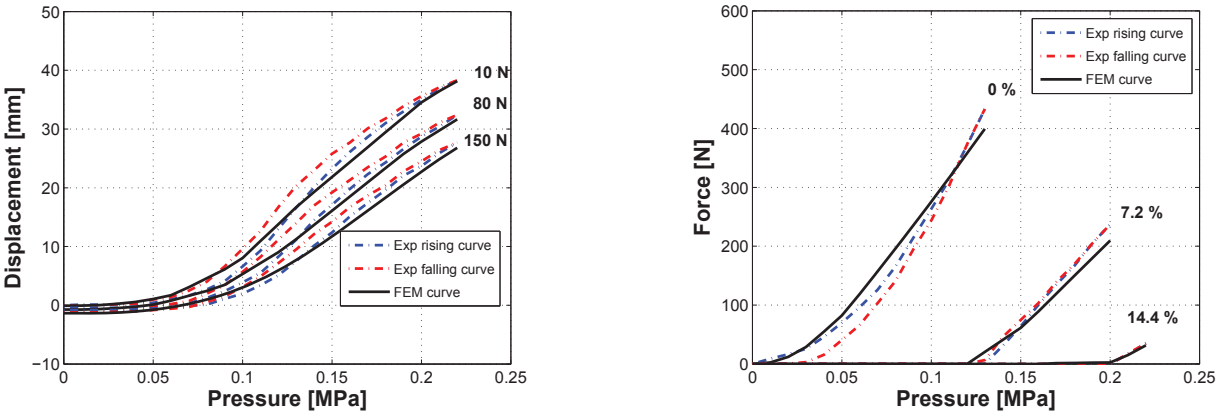

Fig. 8. Comparison between the behaviors of the experimental prototype and the finite element model for the four-segment muscle: isotonic and isometric tests.

expressed as the ratio of the contraction length to the resting length ($\Delta L_m/L_{m0}$), i.e., 0%, 7.2%, and 14.4%, is a parameter.

Analysis of the results leads to the following findings.

- The experimental curves show a hysteretic behavior of the muscle: two distinct curves that indicate the increase and decrease in pressure inside the muscle. This behavior does not depend on the number of segments but on the deformation. The greater the deformation, the greater is the area enclosed by the experimental curves. The behavior of the material of the wires also has an influence on the hysteretic behavior. A hardening behavior too is observed: that is, the stiffness increases with deformation. The hysteresis is due to viscoelastic phenomena [41] that result in time-dependent behaviors: in this case, the material deforms over time under a constant load or for a constant displacement, leading to a decrease in its own elastic reaction over time.
- For all isotonic curves, comparison of the experimental and model curves shows that both sets have equal concavity. However, the displacement values show better agreement for the muscle with four segments than for the muscle with three segments.
- The above observations are also true for the isometric curves. The graphs show a better response to increasing contraction.
- The graphs show that the pneumatic muscle has good performance. The three-segment muscle shows the maximum contraction ranging from 18.1% for the resting length (load 10 N) to 14.8% (with load at 150 N) at 2.2 bar pressure, and the maximum force of 558 N at zero contraction ($L = L_{m0}$) to 127 N with a contraction of 14.4% ($L = [1 - 0.144]L_{m0}$). The four-segment muscle shows the maximum contraction ranging from 15.3% (load 10 N) to 11.1% (150 N) at 2.2 bar pressure, and the maximum force of 433 N at zero contraction ($L = L_{m0}$) to 35 N for 14.4% contraction ($L = [1 - 0.144]L_{m0}$). The errors are mainly due to the hardening of the wires. Note that initially, the prototype is less rigid than the model, while as the deformation increases, the prototype becomes more rigid. This is because the mathematical formulation of the truss elements can model only linear materials with stiffness described by only one constant.

3. Design Procedure

As previously mentioned, the behavior of pneumatic muscles is strongly nonlinear because of the nonlinear behavior of the rubber and because of the large deformations. Consequently, it is difficult to design the dimensions of these actuators. The numerical model proposed and experimentally validated in this study was used to perform a sensitivity analysis to show the influence of major project parameters on muscle performance [44]. Subsequently, a procedure for estimating the dimensions of the muscle was proposed. This procedure is based on the design graphs that correlate design parameters with performance for muscle diameters of 12–70 mm and lengths of 85–250 mm.

The process of development of another design procedure for the muscle for a more general use is also presented in the following subsection. In this procedure, dimensional analysis was used.

Through this approach, three dimensional parameters were identified, and correlation graphs were reduced to one that contains more information than the previous ones. The graph was obtained by linear interpolation of the data obtained from a limited number of finite elements models.

The results obtained with interpolated data are in agreement with those of the numerical model.

3.1. Dimensional Analysis

As known from [45], the result of a dimensional analysis is a complete set of dimensional parameters that describe the physical process in the analysis. In the present case, the dimensional analysis helped construct a single correlation graph between the design parameters, performance parameters, and control parameters, thus simplifying the previously used procedure to estimate the size.

The first step in the analysis is to list all the important parameters for muscle behavior. Subsequently, the dimensions of these parameters are introduced and processed to obtain the dimensional parameters. The behavior of pneumatic muscles depends on various physical parameters: the material of the tube, material of the wires, number of wires (N_t), number of rings (N; the number of segments is $N+1$), muscle resting diameter (Φ_0), length of the resting muscle (L_{m0}), and tube thickness (s).

The tube was made of silicone rubber, and the wires were made of fiberglass.

The performance parameters are the muscle contraction (ΔL_m), developed force (F), and diameter deformation ($\Delta\Phi$). Moreover, another variable, namely, pressure P, is considered the control variable.

A sensitivity analysis was performed to identify the most important design parameters and their effect on muscle behavior [9]. In order to obtain correlation graphs that are simple for practical use, an attempt was made to reduce the number of parameters involved.

Table 2 lists the parameters considered in the dimensional analysis and their dimensions. With regard the length of the muscle, the analysis involves the length of a single segment of muscle L_0, instead of the length of the muscle $L_{m0} = (N+1) \times L_0$, because the use of L_0 allows better formulation of the procedure.

Table 2. List of relevant variables and their dimensions (M = mass, L = length, T = time).

variable		dimension
pressure	P	$\frac{M}{LT^2}$
resting diameter	Φ_0	L
resting length	L_0	L
contraction	ΔL	L
traction force	F	$\frac{ML}{T^2}$

Some considerations were made with regard to the parameters that were not included in the list of important parameters. Ideally, the thickness of the tube should be minimum as the elastic energy stored in the muscle rubber is dependent on the thickness; this stored energy is detrimental in terms of the external work done by the muscle. The thickness of the tube determines the circumferential stiffness of the muscle: the greater the thickness, the less is the contraction. Moreover, it is important that the pipe thickness guarantees the pneumatic seal. Therefore, the thickness (s) was set as 0.1 mm, which can be considered as the ideal value.

The materials were the same as those used in the models presented in the previous sections – that is, the silicone rubber described by the first-order Mooney-Rivlin model characterized by the two constants $C_{10} = 0.0694$ and $C_{01} = 0.0628$, and 40 fiberglass wires of 0.75 mm diameter.

The rubber tube had a Young's modulus $E_t = 70,000$ MPa.

The number of rings (N) was not considered in the dimensional analysis as the procedure focused on estimating the dimensions of a single segment muscle. The total contraction and resting length of a muscle with $N+1$ segments will be given by the parameters relative to the single segment muscle multiplied by the number of segments ($N+1$).

Finally, the variation in diameter $\Delta\Phi$ was not included in the dimensional analysis because by considering a constant curvature for the muscle profile and by simple geometric considerations, $\Delta\Phi$ could be well approximated as $\Delta\Phi = 2L_0/\pi$.

For the dimensional analysis, the condition of dimensional homogeneity is adopted [44]. The relation between the parameters can be expressed as

$$f(P, \Phi_0, L_0, \Delta L, F) = 0.$$

This relationship must be dimensionally homogeneous, i.e., it must be possible to form dimensional products π

Table 3. Dimensional analysis results.

by	yields	dimensionless number
$b=e=0$ $d=1$	$a=0$ $c=-1$	$\pi_1=\dfrac{\Delta L}{L_0}$
$a=d=0$ $b=1$	$c=-1$ $e=0$	$\pi_2=\dfrac{\Phi_0}{L_0}$
$b=d=0$ $a=1$	$c=2$ $e=-1$	$\pi_3=\dfrac{P\cdot {L_0}^2}{F}$

with these quantities:

$$\pi = P^a \cdot \Phi_0^b \cdot L_0^c \cdot \Delta L^d \cdot F^e$$

Further, by introducing the dimensions of the parameters, π is obtained as follows:

$$\pi = \left[\frac{M}{LT^2}\right]^a \cdot [L]^b \cdot [L]^c \cdot [L]^d \cdot \left[\frac{ML}{T^2}\right]^e$$

Then, for the three dimensions, we have the following relations:

$$\begin{cases} +a+e=0 & \text{for } M \\ -2a-2e=0 & \text{for } T \\ -a+b+c+d+e=0 & \text{for } L \end{cases}$$

The first and second equations are linearly dependent, so the number of useful relationships is two; however, there are five unknowns. Therefore, three dimensionless quantities can be defined. Knowledge of the studied phenomenon is useful for defining the dimensionless groupings.

Thus, three dimensionless numbers, π_1, π_2, and π_3, as listed in **Table 3** are obtained.

The number π_1 includes a functional parameter, namely, muscle contraction ΔL.

The number π_2 includes only design parameters, namely, the resting diameter Φ_0 and resting length L_0 of the muscle. The third quantity π_3 includes a performance parameter F and a control parameter P.

3.2. Design of the Pneumatic Muscle

Relationships between the three groups of π were evaluated using the finite element model; this was done according to a plan for which 27 models were prepared. The use of 27 models was considered sufficient to provide a description of the phenomenon. These data are presented in **Table 4**.

The pressure levels considered are those that bring the muscle with nearly no load (load = 1 N) to a maximum circumferential deformation of 180%, which is an acceptable level for the structural integrity of the silicone rubber considered. **Table 4** lists the data used to build the correlation graph. In the correlation graph, shown in **Fig. 9**, $(P\cdot {L_0}^2)/F$ is used as a parameter, while $\Delta L/L_0$ and Φ_0/L_0 are the coordinates of the Cartesian axes.

The curves allow estimating the dimensions of the pneumatic muscle with $0.25 < \Phi_0/L_0 < 0.5$. The correlation graph was validated by finite element models, as presented in **Table 5**, using data very far from those used to construct the graph. This validation showed a maximum error of 3.36%.

By using the dimensional correlation graph and the expression for $\Delta\Phi$, the performance for each combination of the design parameters could be estimated.

With reference to **Fig. 10**, the design procedure is described below.

Table 4. Data used to construct the correlation graph.

Φ_0 [mm]	L_0 [mm]	P [MPa]	F [N]	Φ_0/L_0	ΔL [mm]	$\Delta L/L_0$	$\frac{P\cdot {L_0}^2}{F}$
30	120	0.2	1	0.25	51.96	0.433	2880
30	80	0.45	1	0.375	30.98	0.387	2880
30	60	0.8	1	0.5	20.7	0.345	2880
30	120	0.2	10	0.25	51.66	0.43	288
30	80	0.45	10	0.375	30.84	0.386	288
30	60	0.8	10	0.5	20.67	0.344	288
30	120	0.2	100	0.25	49.05	0.409	28.8
30	80	0.45	100	0.375	29.52	0.369	28.8
30	60	0.8	100	0.5	19.90	0.332	28.8
30	120	0.2	400	0.25	41.20	0.343	7.2
30	80	0.45	400	0.375	25.47	0.3184	7.2
30	60	0.8	400	0.5	17.53	0.292	7.2
30	120	0.2	800	0.25	32.37	0.27	3.6
30	80	0.45	800	0.375	20.84	0.26	3.6
30	60	0.8	800	0.5	14.77	0.246	3.6
30	120	0.2	1200	0.25	25.06	0.209	2.4
30	80	0.45	1200	0.375	16.97	0.212	2.4
30	60	0.8	1200	0.5	12.41	0.207	2.4
30	120	0.2	1600	0.25	19.08	0.159	1.8
30	80	0.45	1600	0.375	13.71	0.171	1.8
30	60	0.8	1600	0.5	10.41	0.173	1.8
30	120	0.2	2000	0.25	14.28	0.119	1.44
30	80	0.45	2000	0.375	11.02	0.138	1.44
30	60	0.8	2000	0.5	8.71	0.145	1.44
30	120	0.2	2400	0.25	10.578	0.088	1.2
30	80	0.45	2400	0.375	8.83	0.11	1.2
30	60	0.8	2400	0.5	7.28	0.12	1.2

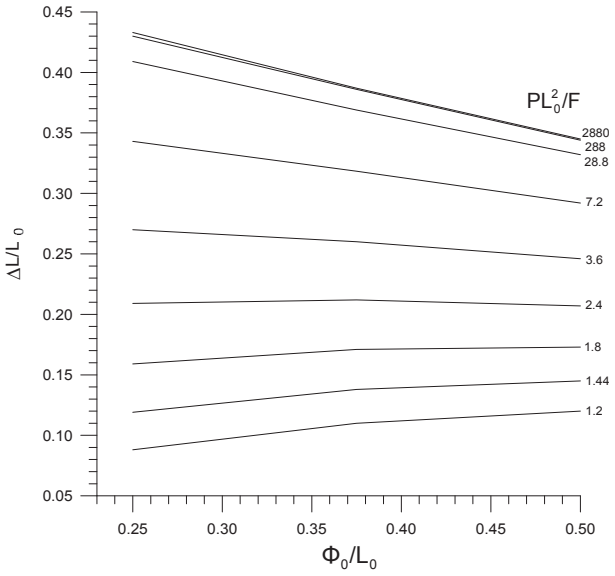

Fig. 9. Dimensionless correlation graph (dcg).

Table 5. Simulated test plan used to validate the dimensionless correlation graph.

Φ_0 [mm]	L_0 [mm]	Φ_0/L_0	$\Delta L/L_0$ dcg	PL^2/F	F [N]	P [MPa]	ΔL [mm]	$\Delta L/L_0$ FEM	Err [%]
20	80	0.25	0.430	288	10	0.45	34.52	0.432	0.46
40	160	0.25	0.430	288	10	0.112	68.79	0.430	0.00
23	92	0.25	0.430	288	10	0.34	39.67	0.431	0.23
30	100	0.3	0.413	288	10	0.288	41.2	0.412	0.24
30	100	0.3	0.266	3.6	800	0.288	26.69	0.267	0.37
30	100	0.3	0.266	3.6	400	0.144	26.53	0.265	0.38
30	100	0.3	0.266	3.6	200	0.072	26.25	0.262	1.5
70	233	0.3	0.266	3.6	800	0.053	61.62	0.264	0.75
70	233	0.3	0.332	7.2	400	0.053	77.18	0.331	0.3
70	233	0.3	0.332	7.2	800	0.106	77.55	0.333	0.3
40	93	0.43	0.307	7.2	400	0.333	28.49	0.306	0.33
40	93	0.43	0.307	7.2	200	0.166	28.40	0.305	0.66
40	93	0.43	0.171	1.8	500	0.104	15.89	0.171	0.00
40	93	0.43	0.367	288	10	0.333	34.1	0.366	0.27
25	100	0.25	0.343	7.2	100	0.072	33.9	0.339	1.18
25	100	0.25	0.119	1.44	500	0.072	11.52	0.115	3.36

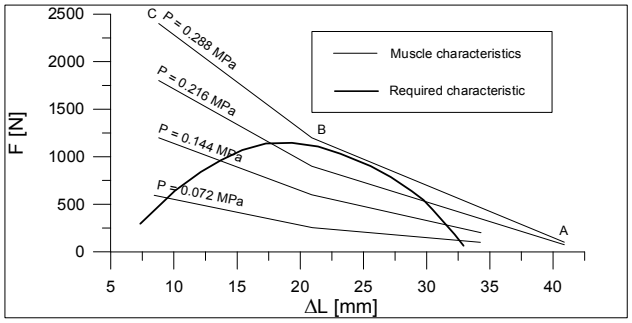

Fig. 10. Muscle characteristics obtained by means of the dimensional correlation graph for $\Phi_0 = 25$ mm and $L_0 = 100$ mm.

The required muscle performance, that is, the force F as a function of the contraction ΔL_m is shown in the figure (bold line). Further, the maximum permissible diameter is known for the application.

The designer chooses a set of values for the design parameters Φ_0, L_{m0}, s, and N. Using the correlation graph, the static muscle characteristics (curves that provide F as a function of ΔL_m at constant pressure) are obtained. The designer then verifies that the best static characteristics lie over the required characteristics.

The steps to obtain the static muscle characteristics are described below:

1) Choose a set of values for Φ_0, L_{m0}, s, and N.

2) Calculate the length of the single segment $L_0 = L_{m0}/(N+1)$ and Φ_0/L_0.

3) Entering Φ_0/L_0 into the dimensional correlation graph yields the highest value of $\Delta L/L_0$ corresponding to the maximum value of the dimensional parameter $(P \cdot L_0^2)/F$; then, derive ΔL and apply the correction for thickness s: $\Delta Lc = \Delta L - K_S \times L_0$. This equation was derived after assuming a relationship that was verified by numerical simulations. See **Table 6** for K_S values.

Table 6. Correction factors for the thickness.

s [mm]	1	2	4
K_S	0.11	0.22	0.44

4) By assigning $F = 1$ N, determine pressure P that defines the corresponding muscle characteristic.

5) Obtain the maximum ΔL_m for the muscle by using the relation $\Delta L_m = \Delta Lc \times (N+1)$. F and ΔL_m represent the first point of the best static characteristic (point A in **Fig. 10**).

6) Use Φ_0/L_0 in the dimensional correlation graph to obtain $\Delta L/L_0$ corresponding to the intermediate values of $(P \cdot L_0^2)/F$. Determine force F (P is known from step 4), and as done for the previous point, determine ΔL_m. This defines point B in **Fig. 10**.

7) Enter Φ_0/L_0 in the dimensional correlation graph to get $\Delta L/L_0$ corresponding to the minimum value of $(P \cdot L_0^2)/F$; obtain the force F and ΔL_m that define the point C in **Fig. 10**.

Considering a linear pattern between the obtained points, the characteristic of the muscle is traced. Further, verification is performed to determine whether the characteristic meets the required performance and whether the value for the maximum $\Delta\Phi$ is acceptable. If not, the procedure is repeated from step 1. If these conditions are met, following the steps 3), 5), 6), and 7), the other characteristics are obtained for other values corresponding to pressure lower than the already obtained P. These characteristics will be useful in the design phase of the control system of the muscle. **Fig. 10** shows the static characteristics for a single segment muscle with $L_{m0} = L_0 = 100$ mm

and $\Phi_0 = 25$ mm, without correction for the thickness, as obtained using the proposed procedure.

The correction factor K_S in **Table 6** for the maximum and minimum values of $\Delta Lc/L_0$ introduces an error of 6% and 20%, respectively, for $s = 4$ mm; 5% and 11%, respectively, for $s = 2$ mm; and 2% and 6%, respectively, for $s = 1$ mm.

4. Conclusion

This work presented the numerical modeling and experimental validation of a pneumatic muscle actuator based on the idea of a research group at Warsaw University. The actuator was designed and modeled numerically, and the model was validated by using an experimental prototype made in the laboratory. The numeric model was built with the code for finite elements based on Mooney-Rivlin's model for rubber. Experimental validation was based on isotonic and isometric tests. The tests were conducted for two versions of the actuator with three and four segments. The results of the comparison between the model and the prototypes are presented and discussed. The results show a good agreement, indicating that the numerical model can be used to predict muscle behavior. The described model was used to develop a design procedure for the pneumatic muscle actuator. This is based on a single design graph with three variables. The variables were defined by dimensional analysis, leading to the definition of three parameters. The curves were defined by the proposed finite element models. The correlation graph was numerically validated by using the finite element models with a wide range of input parameters. Finally, an example of estimation of the size of a pneumatic muscle is presented.

References:

[1] M. G. Antonelli, S. Alleva, P. Beomonte Zobel, and F. Durante, "A Methodology for the Development of an Active Ankle Prosthesis," Int. J. of Mechanical Engineering and Technology, Vol.9, No.2, pp. 221-234, 2018.

[2] F. Durante, P. Beomonte Zobel, and T. Raparelli, "Development of an active orthosis for inferior limb with light structure," Proc. of RAAD2017, July 21-23, Torino, Italy, 2012, pp. 783-791, 2012.

[3] N. Koceska, S. Koceski, F. Durante, P. Beomonte Zobel, and T. Raparelli, "Control architecture of a 10 DOF lower limbs exoskeleton for gait rehabilitation," Int. J. of Advanced Robotic Systems, Vol.10, No.168, doi: 10.5772/55032, 2013.

[4] J. Fryman and B. Matthias, "Safety of Industrial Robots: From conventional to Collaborative Applications," Proc. of ROBOTIK 2012, 7th Conf. on Robotics, May 21-22, Munich, Germany, 2012.

[5] A. Bicchi and G. Tonietti, "Fast and soft arm tactics: dealing with the safety-performance tradeoff in robot arms design and control," IEEE Robotics and Automation, Vol.11, No.2, pp. 22-33, 2004.

[6] H. F. Schulte, "The characteristic of the McKibben artificial muscle," National Academy of Sciences, National Research Council (Eds.), The Application of External Power in Prosthetics and Orthotics (Publication 874, Appendix H), Washington, DC: National Academy of Sciences, National Research Council, pp. 94-115, 1962.

[7] J. M. Winters, "Braided artificial muscles: mechanical properties and future uses in prosthetics/orthotics," Proc. of the RESNA 13th annual conf., Washington, DC, June 15-20, pp. 173-174, RESNA Press, 1990.

[8] D. G. Caldwell, A. Razak, and M. J. Goodwin, "Braided pneumatic muscle actuators," Proc. of the IFAC Conf. on intelligent autonomous vehicles, Southampton, April 18-21, pp. 507-512, Pergamon, 1993.

[9] C. P. Chou and B. Hannaford, "Measurement and modelling of McKibben pneumatic artificial muscles," IEEE Trans. on Robotics and Automation, Vol.12, No.1, pp. 90-102, 1996.

[10] G. Belforte, G. Eula, A. Ivanov, T. Raparelli, and S. Sirolli, "Presentation of textile pneumatic muscle prototypes applied in an upper limb active suit experimental model," The J. of Textile Institute, doi: 10.1080/00405000.2017.1368111, 2017.

[11] G. B. Immega, "ROMAC actuators for micro robots," Proc. of micro robotics and teleoperators workshop, IEEE Robotics and Automation Council, Hyannis, MA, November 9-11, 1987.

[12] H. A. Baldwin, "Realizable models of muscle function," Proc. of the first rock biomechanics symposium, New York, April 5-6, pp. 139-148, Springer, 1967.

[13] J. N. Marcinčin, J. Smrček, and J. Niznik, "Bioactuators – most efficient actuators for biomechanics," Proc. of the 7th Int. IMEKO TC-13 on measurement in clinical medicine "Model Based Biomeasurement," Stara Lesna, September 6-9, pp. 369-371, P. Kneppo and M. Tysler (Eds.), 1995.

[14] F. Daerden and D. Lefeber, "Pneumatic artificial muscles: actuators for robotics and automation," European J. of Mechanical and Environmental Engineering, Vol.47, No.1, pp. 11-21, 2002.

[15] D. Villegas, M. Van Damme, B. Vanderborght, P. Beyl, and D. Lefeber, "Third-generation pleated pneumatic artificial muscle for robotic applications: development and comparison with McKibben muscle," Advanced Robotics, Vol.26, No.11-12, pp. 1205-1227, 2012.

[16] T. Noritsugu, M. Takaiwa, and D. Sasaki, "Development of a pneumatic rubber artificial muscle for human support applications," Proc. of the 9th Scandinavian int. conf. on fluid power, Linkoping, June 1-3, 2005.

[17] M. G. Antonelli, P. B. Zobel, P. Raimondi, T. Raparelli, and G. Costanzo, "An innovative brace with pneumatic thrusts for scoliosis treatment," Int. J. of Design & Nature and Ecodynamics, Vol.5, No.4, pp. 1-14, 2010.

[18] G. Belforte, G. Eula, A. Ivanonv, and S. Sirolli, "Soft pneumatic actuators for rehabilitation," Actuators, Vol.3, pp. 84-106, 2014.

[19] M. G. Antonelli, P. Beomonte Zobel, F. Durante, and F. Gaj, "Development and testing of a grasper for NOTES powered by variable stiffness pneumatic actuation," Int. J. of Medical Robotics and Computer Assisted Surgery, doi: 10.1002/rcs.1796, 2016.

[20] A. Morecki, "Polish artificial pneumatic muscles," Proc. of the 4th Int. Conf. on climbing and walking robot, Karlsruhe, September 24-26, 2001.

[21] N. Tsagarakis and D. G. Caldwell, "Improved modelling and assessment of pneumatic muscle actuators," Proc. of int. conf. on robotics and automation, San Francisco, CA, April 24-28, pp. 3641-3646, IEEE, New York, 2000.

[22] M. Doumit, A. Fahim, and M. Munro, "Analytical modelling and experimental validation of the braided pneumatic muscle," IEEE Trans. Robotics, Vol.25, No.6, pp. 1282-1291, 2009.

[23] F. Sorge and M. Cammalleri, "A theoretical approach to pneumatic muscle mechanics," Proc. of IEEE/ASME int. conf. on advanced intelligent mechatronics, Wollongong, NSW, Australia, July 9-12, pp. 1021-1026, IEEE, New York, 2013.

[24] G. K. Klute and B. Hannaford, "Fatigue characteristic of McKibben artificial muscle actuators," Proc. of int. conf. on intelligent robots and systems conf., Victoria, BC, Canada, October 13-17, pp. 1776-1781, IEEE, New York, 1998.

[25] D. A. Kingsley and R. D. Quinn, "Fatigue life and frequency response of braided pneumatic actuators," Proc. of IEEE robotics and automation conf., Washington, DC, May 11-15, pp. 2830-2835, IEEE, New York, 2002.

[26] G. Belforte, T. Raparelli, and S. Sirolli, "A novel geometric Formula for Predicting Contractile Force in McKibben Pneumatic Muscles," Int. J. of Automation Technology, Vol.11, No.3, pp. 368-377, 2017.

[27] S. Wakimoto, K. Suzumori, and J. Takeda, "Flexible artificial muscle by bundle of McKibben fiber actuators," Proc. of IEEE/ASME int. conf. on advanced intelligent mechatronics, Budapest, July 3-7, pp. 457-462, New York: IEEE, 2011.

[28] T. Nozaki and Y. Noritsugu, "Motion analysis of McKibben type pneumatic rubber artificial muscle with finite element method," Int. J. of Automation Technology, Vol.8, No.2, pp. 147-158, 2014.

[29] M. G. Antonelli, P. B. Zobel, F. Durante, and T. Raparelli, "Numerical modelling and experimental validation of a McKibben pneumatic muscle actuator," J. of Intelligent Material Systems and Structures, doi: 10.1177/1045389X17698245, 2017.

[30] D. Sasaki, T. Noritsugu, and M. Takaiwa, "Development of Active Support Splint Driven by Pneumatic Soft Actuator (ASSIST)," J. of Robotics and Mechatronics, Vol.16, No.5, pp. 497-503, 2004.

[31] T. Noritsugu, D. Sasaki, M. Kameda, A. Fukunaga, and M. Takaiwa, "Wearable Power Assist Device for Standing Up Motion Using Pneumatic Rubber Artificial Muscles," J. of Robotics and Mechatronics, Vol.19, No.6, pp. 619-628, 2007.

[32] H. Kobayashi, A. Takamitsu, and T. Hashimoto, "Muscle Suit Development and Factory Application," Int. J. of Automation Technology, Vol.3, No.6, pp. 709-715, 2009.
[33] Y. Muramatsu, H. Kobayashi, Y. Sato, H. Jiaou, T. Hashimoto, and H. Kobayashi, "Quantitative Performance Analysis of Exoskeleton Augmentation Devices – Muscle Suit – for Manual Worker," Int. J. of Automation Technology, Vol.5, No.4, pp. 559-567, 2011.
[34] H. Kobayashi, T. Hashimoto, S. Nakayama, and K. Irie, "Development of an Active Walker and its Effect," J. of Robotics and Mechatronics, Vol.24, No.2, pp. 275-283, 2012.
[35] X. Li, T. Noritsugu, M. Takaiwa, and D. Sasaki, "Design of Wearable Power Assist Wear for Low Back Support Using Pneumatic Actuators," Int. J. of Automation Technology, Vol.7, No.2, pp. 228-236, 2013.
[36] K. Nazarczuk, "Teorie sztucznych napedow miesniowych i jej zastosowanie do syntezy i sterowanie biomanipulatorow," Ph.D. thesis, Warsaw Politecnical School, 1970.
[37] T. Nakamura, "Experimental Comparisons between McKibben Type Artificial Muscles and Straight Fibers Type Artificial Muscles," Proc. of SPIE Int. Conf. on Smart Structures, Devices and Systems III, 2006.
[38] C. Ferraresi, W. Franco, and A. M. Bertetto, "Flexible Pneumatic Actuators: A comparison between the McKibben and the Straight Fibres Muscles," J. of Robotics and Mechatronics, Vol.13, No.1, pp. 56-63, 2001.
[39] H. Tomori and T. Nakamura, "Theoretical Comparison of McKibben-Type Artificial Muscle and Novel Straight-Fiber-Type Artificial Muscle," Int. J. of Automation Technology, Vol.5, No.4, pp. 544-550, 2011.
[40] T. Raparelli, P. B. Zobel, and F. Durante, "The Design of a 2-dof Robot for Functional Recovery Therapy driven by Pneumatic Muscles," paper RD-078, RAAD 2001, 10th Int. Workshop on ROBOTICS IN ALPE – ADRIA – DANUBE REGION, Vienna, May 16-18, 2001.
[41] J. D. Ferry, "Viscoelastic Properties of Polymers," John Wiley & Sons, Inc., New York, 1980.
[42] T. Raparelli, F. Durante, and P. Beomonte Zobel, "Numerical modelling and experimental validation of a pneumatic muscle actuator," Proc. 4th JHPS Int. Symposium on Fluid Power, Tokyo '99, November 15-17, 1999.
[43] T. Raparelli, P. B. Zobel, and F. Durante, "On the design of pneumatic muscle actuators," 2nd Int. Fluidtechnisches Kolloquium, March 16-17, Dresda, 2000.
[44] T. Raparelli, F. Durante, and P. B. Zobel, "Una metodologia di progetto di attuatori a muscolo pneumatico," XIV Congresso Nazionale AIMETA, Como, Italy, October, 1999.
[45] M. Zlokarnik, "Dimensional Analysis and Scale-up in Chemical Engineering," Springer-Verlag, Berlin, 1991.

Name:
Francesco Durante

Affiliation:
Department of Industrial and Information Engineering and Economics (DIIIE), Università dell'Aquila

Address:
DIIIE, Via Giovanni Gronchi, 18 67100 L'Aquila, Italy

Brief Biographical History:
1992 Master degree in Mechanical Engineering
1997 Ph.D. in Quality Engineering
2002-2017 Assistant Professor, Applied Mechanics, Università dell'Aquila

Main Works:
• "Numerical modelling and experimental validation of a McKibben pneumatic muscle actuator," J. of Intelligent Material Systems and Structures, doi: 10.1177/1045389X17698245, 2017.
• "Control architecture of a 10 DOF lower limbs exoskeleton for gait rehabilitation," Int. J. of Advanced Robotic Systems, Vol.10, art. No.68, 2013.
• "Design of a parallel robot actuated by shape memory alloy wires," Materials Trans., Vol.43, No.5, pp. 1015-1022, 2002.

Name:
Michele Gabrio Antonelli

Affiliation:
Department of Industrial and Information Engineering and Economics (DIIIE), Università dell'Aquila

Address:
DIIIE, Via Giovanni Gronchi, 18 67100 L'Aquila, Italy

Brief Biographical History:
2001 Master degree in Mechanical Engineering
2005 Ph.D. in Mechanical Engineering
2005-2017 Research Assistant, Applied Mechanics, Università dell'Aquila

Main Works:
• "Numerical modelling and experimental validation of a McKibben pneumatic muscle actuator," J. of Intelligent Material Systems and Structures, doi: 10.1177/1045389X17698245, 2017.
• "Development and testing of a grasper for NOTES powered by variable stiffness pneumatic actuation," Int. J. of Medical Robotics and Computer Assisted Surgery, doi: 10.1002/rcs.1976, 2017.
• "Use of MMG signals for the control of powered orthotic devices: development of a rectus femoris measurement protocol," Assist. Technol., Vol.21, No.1, pp. 1-12, 2009.

Name:
Pierluigi Beomonte Zobel

Affiliation:
Department of Industrial and Information Engineering and Economics (DIIIE), Università dell'Aquila

Address:
DIIIE, Via Giovanni Gronchi, 18 67100 L'Aquila, Italy

Brief Biographical History:
1990- Assistant Professor, Università dell'Aquila
2000- Associate Professor, Università dell'Aquila

Main Works:
• "An innovative brace with pneumatic thrusts for scoliosis treatment," Int. J. of Design & Nature and Ecodynamics, Vol.5 No.4, pp. 354-367, 2010.
• "Development of a New Harvesting Module for Saffron Flower Detachment," Romanian Review of Precision Mechanics, Optics & Mechatronics, Vol.39, pp. 163-168, 2011.

Name:
Terenziano Raparelli

Affiliation:
Professor, Department of Mechanical and Aerospace Engineering (DIMEAS), Politecnico di Torino

Address:
DIMEAS, Politecnico di Torino, Corso Duca degli Abruzzi 24, 10129, Torino, Italy

Brief Biographical History:
1983- Joined Politecnico di Torino
1992- Associate Professor, Politecnico di Torino
1994- Full Professor, University of L'Aquila
1999- Full Professor, Politecnico di Torino

Main Works:
• Fluid automation: pneumatic systems and components, pneumatics control
• Tribology: gas bearings, friction and wear in seals
• Robotics: mobile and fixed robots, wrists, grippers
• Bioengineering: exoskeleton, pneumatic muscles

Membership in Academic Societies:
• Society of Tribologists and Lubrication Engineering (STLE)
• International Federation for the Promotion of Mechanism and Machine Science (IFToMM)
• Italian Association of Theoretical and Applied Mechanics (AIMETA)